ICA 2016 BUENOS AIRES
Buenos Aires – 5 to 9 September 2016
Acoustics for the 21st Century...

PROCEEDINGS of the 22nd International Congress on Acoustics

Numerical Techniques: Paper ICA2016-210

A boundary integral operator method for modelling uncertainties in vibro-acoustics

Janis Bajars[(a)], **David Chappell**[(b)]

[(a)]Nottingham Trent University, UK, janis.bajars@ntu.ac.uk
[(b)]Nottingham Trent University, UK, david.chappell@ntu.ac.uk

Abstract

Dynamical Energy Analysis (DEA) is an approach for studying the vibro-acoustic response of complex systems in the high frequency limit. The method has been extended to industrial scale applications using an efficient implementation on meshes known as Discrete Flow Mapping. DEA is a deterministic boundary transfer operator method for the modelling of phase-space densities (or ray densities) arising in the ray-tracing approximation of a linear wave problem. In this work, we investigate extensions of the DEA approach to stochastic boundary transfer operator methods by replacing the deterministic description of the ray flow with a probabilistic flow map incorporating various sources of uncertainty. We will present efficient numerical approaches with relevance to high-frequency vibro-acoustic wave problems.

Keywords: Boundary Integral Methods; Ray Tracing; Parametric Uncertainties

A boundary integral operator method for modelling uncertainties in vibro-acoustics

1 Introduction

Boundary integral formulations for propagating particle or ray densities along ray trajectories in computer graphics applications are often termed the rendering equation [1]. Consequently the rendering equation lies at the heart of a wide variety of algorithms, both for applications in computer graphics [1] and beyond [2, 3, 4]. The point of departure for this study stems from the observation that the rendering equation may be formulated using deterministic transfer operators of Frobenius-Perron (FP) type [4, 5]. Replacing the deterministic transfer operator with a stochastic one results in a boundary integral formulation for stochastic propagation of ray densities. The simplest implementation of a stochastic treatment is to assume that rays propagate uniformly with equal probability of all admissible propagated ray vectors. This formulation is known as the radiosity method (with Lambertian reflection) in the room acoustics community [2, 3]. A more widely applicable implementation arises if one assumes that the mapped ray vector is normally distributed, with mean given by the associated deterministic dynamics. The resulting stochastic evolution operator will be of Fokker-Planck type as discussed in [6, 7]. The choice of variance in this approach allows the model to be tuned to the level of uncertainty prescribed by the application. Example applications arise in fluid dynamics [8], weather forecasting [9], linear wave dynamics or in general in describing the evolution of phase-space densities of a dynamical system.

In this work, we present a family of boundary integral approaches based on the use of stochastic evolution operators. We will discuss how a scaled and truncated Gaussian probability distribution leads to an integral equation model that interpolates between uniformly stochastic and deterministic propagation. One can view the small variance limit as approximating a (multi-dimensional) delta distribution by a sequence of Gaussians of decreasing width. Scaling is necessary to prevent the uncertainty from introducing artificial energy losses into the system due to truncation of the infinite tails of the Gaussian. We then detail the modelling of two specific sources of vibro-acoustic uncertainty within this stochastic evolution operator framework; namely, we describe the modelling of (i) uncertain (or rough surface) reflections and (ii) uncertainties in the location of a point source driving the system. Once the variance has been prescribed according to the (estimated) level of uncertainty in the model, an appropriate numerical solution approach can be applied. These are typically the usual approaches for numerically solving integral equations, such as the Nyström, collocation or Galerkin methods. We then present the results of some supporting numerical simulations to demonstrate the practical application of the above described methodology.

2 Boundary integral operator model for the stochastic propagation of densities

2.1 Governing boundary integral equations

Consider phase-space in two-dimensions with $\mathbf{r} \in \mathbb{R}^2$ the spatial position and $\mathbf{p} \in \mathbb{R}^2$ is the momentum or slowness vector. Let Ω denote a finite two-dimensional domain with an associated speed of propagation c. The Hamiltonian $\hat{H} = c|\mathbf{p}| = 1$ therefore describes the ray trajectories within Ω between reflections due to hitting the boundary $\Gamma = \partial\Omega$. We write the phase-space coordinates on the boundary of Ω as $X = (s, p)$, where s is an arc-length parametrisation of Γ and $p = c^{-1}\sin(\theta)$ is the tangential component of the momentum vector $\mathbf{p}$ at the point s, where $\theta \in (-\pi/2, \pi/2)$ is the angle between the trajectory leaving the boundary at s and the normal vector to Γ (also at s).

The stochastic propagation of a density ρ through phase-space is described by an operator of the form

$$\mathscr{L}_\sigma \rho(X) = \int_Q f_\sigma(X - \varphi(X'))\rho(X')\,\mathrm{d}X'. \tag{1}$$

Here $Q = \Gamma \times (-c^{-1}, c^{-1})$ denotes the phase-space on the boundary and $\varphi : Q \to Q$ defines the boundary flow map, which maps a vector in Q to another vector in a subset of Q, leading to a deterministic evolution of the form $\varphi(X') = X$, where $X' = (s', p')$, $X = (s, p)$. Geometrically φ corresponds to the composition of a translation (from s' to s) and a rotation to the direction corresponding to a specular reflection. The kernel of the boundary integral operator (1) is given by a probability density function (PDF) f_σ such that

$$\int_Q f_\sigma(X)\,\mathrm{d}X = 1, \tag{2}$$

and σ is a parameter set controlling its shape.

With reference to applications in vibro-acoustics, this probabilistic behaviour could be attributed to, for example, fluctuations in the wave speed c, roughness of the reflecting surface or uncertainty in the exact position of the boundary or a source term. In the following, we will focus on how such models can be applied to model rough surface reflections and uncertain sources. In all cases we assume that the total energy $\hat{H} = c|\mathbf{p}| = 1$ remains fixed and that the total probability is conserved, that is, condition (2) holds throughout. Note that in contrast to the models considered in [6, 7], the range of integration in the domains considered here is in general bounded, which has implications for the choice of suitable PDFs f_σ. The simplest case is to take $f_\sigma = const$, upon which one arrives at a model describing propagation to all admissible positions and directions with equal probability. The system is thus by definition ergodic and independent of the underlying classical dynamics. In general, we would like to arrive at a stochastic operator which includes both deterministic propagation and the random propagation model described above as limiting cases [10]. In addition, the PDF f_σ needs to obey conditions on the sampling ranges due to the limited range of the boundary map φ. For simplicity we will restrict to convex domains Ω to avoid additional complications due to incorporating visibility functions.

For an initial boundary distribution ρ_0 on Q, the final equilibrium distribution (including contributions from arbitrarily many reflections) may be computed using the following boundary integral equation (see for example [4] and [10]),

$$(I - \mathscr{L}_\sigma)\rho = \rho_0. \tag{3}$$

Note that for the sum over all reflections to converge, energy losses must be introduced into the system, which could take place at the boundaries themselves, or along the trajectories. In general, a weight factor w will be added inside the integral in the definition of $\mathscr{L}_\sigma$ which contains a dissipative term, and for the extension to multiple domains connected at interfaces w will also contain reflection/transmission probabilities at these interfaces.

2.2 On the choice of probability distribution function f_σ

We may interpret the evolution given by the operator in Eq. (1) as originating from a stochastic boundary map φ_σ with added noise, that is,

$$\begin{aligned} \varphi_\sigma(X') &= X \\ &= \varphi(X') + X_\varepsilon, \end{aligned} \tag{4}$$

where $X_\varepsilon = (s_\varepsilon, p_\varepsilon)$ are random variables drawn from the PDF f_σ. Note that s_ε is understood as a shift in counter-clockwise direction. For $X \in Q$ given, we have to ensure that $\varphi(X') = X - X_\varepsilon$ is still in the range of the deterministic map φ; this yields restrictions on the possible values of X_ε and thus on the domain of f_σ.

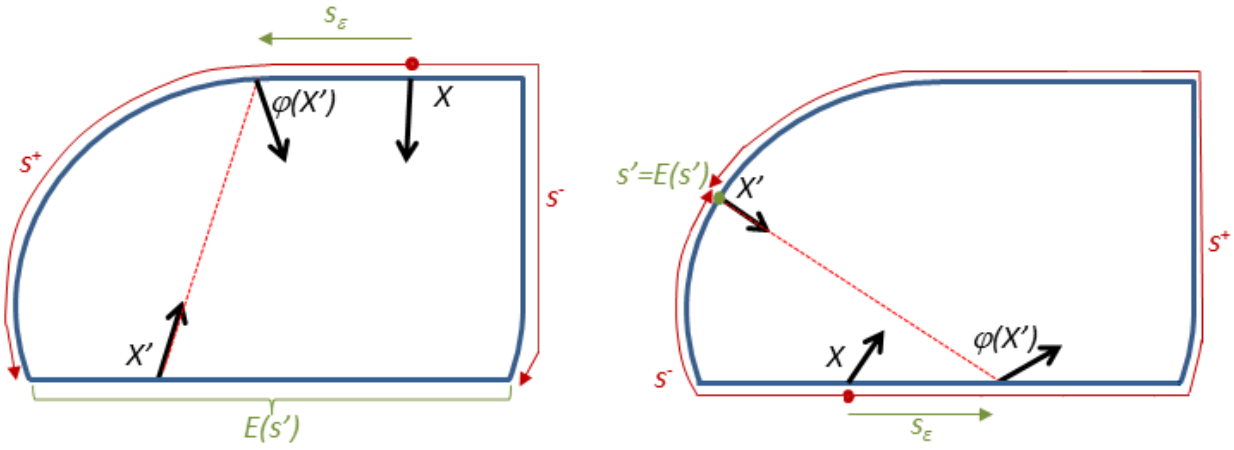

Source: Ref. [10]

Figure 1: **Tracking ray trajectories via a noisy boundary map and truncation limits $s^\pm$ for the random variable s_ε.**

We define $\varphi = (\varphi_s, \varphi_p)$ in terms of its position and momentum components and write the initial coordinate as $X' = (s', p')$. The range of admissible values for $\varphi_s(X')$ is $[0, L) \setminus E(s')$, where $E(s')$ is the (closed) set of all points on the same straight edge as s', see Fig. 1. Note that

for curved edges we set $E(s') = s'$ as shown in the right plot of Fig. 1. Furthermore, we have that $\varphi_p(X') \in (-c^{-1}, c^{-1})$. It is therefore necessary to truncate the ranges from which X_ε are sampled to the ranges where for fixed X, $\varphi(X') \in ([0,L) \setminus E(s') \times (-c^{-1}, c^{-1})$ in Eq. (4). Denoting these truncated ranges by (X^-, X^+) where $X^\pm = [s^\pm, p^\pm]$, the PDF f_σ will have support on $X_\varepsilon \in (X^-, X^+)$ only. The truncated sampling ranges are given as $s^+(s', s) = \min\{x > 0 : s + x \in E(s') \pmod L\}$ and correspondingly $s^-(s', s) = \max\{x < 0 : s + x \in E(s') \pmod L\}$ (see Fig. 1). Likewise in the momentum coordinate, $p^+(p) = c^{-1} - p$ and $p^-(p) = -c^{-1} - p$. Using Heaviside functions we define a cut-off function for restricting the support of f_σ to (X^-, X^+) as follows

$$\chi(X_\varepsilon; X^-, X^+) = (H(s^+ - s_\varepsilon) - H(s^- - s_\varepsilon))(H(p^+ - p_\varepsilon) - H(p^- - p_\varepsilon)). \tag{5}$$

Note that we have omitted the dependence of $s^\pm$ and $p^\pm$ on X' and X for brevity.

Having obtained the domain of the PDF, we can now construct f_σ explicitly; we will derive the PDF from an uncorrelated bivariate Gaussian distribution with mean $\mathbf{0} = [0,0]$ and standard deviation $\sigma = (\sigma_1, \sigma_2)$. A normalized PDF is then obtained by setting

$$f_\sigma(X_\varepsilon; X^-, X^+) = \frac{\chi(X_\varepsilon; X^-, X^+) \exp\left(-\frac{s_\varepsilon^2}{2\sigma_1^2}\right) \exp\left(-\frac{p_\varepsilon^2}{2\sigma_2^2}\right)}{2\pi\sigma_1\sigma_2 \psi_{\sigma_1}(s^-, s^+) \psi_{\sigma_2}(p^-, p^+)}, \tag{6}$$

where the normalization defined through ψ_{σ_1} and ψ_{σ_2} is given as

$$\psi_{\sigma_1}(s^-, s^+) = \frac{1}{2}\left(\operatorname{erf}\left(\frac{s^+}{\sqrt{2}\sigma_1}\right) - \operatorname{erf}\left(\frac{s^-}{\sqrt{2}\sigma_1}\right)\right), \tag{7}$$

and ψ_{σ_2} is defined analogously. The normalisation ensures that the PDF satisfies condition (2) for the truncated sampling ranges specified through χ. Note that the mean and variance of f_σ differs in general from that of the underlying Gaussian distribution, but can be computed from the PDF (6) using standard formulae.

Taking the limit of (6) as $\sigma \to \mathbf{0}$ then the distribution becomes increasingly sharp and the bivariate Gaussian tends to a two-dimensional delta distribution localised around $X_\varepsilon = X - \varphi(X') = \mathbf{0}$, which leads to a deterministic model. Taking the limit as σ_1, and σ_2 go to ∞ and using the leading order asymptotic expansion of the error function about 0 returns a uniform distribution for $s_\varepsilon \in (s^-, s^+)$ and $p_\varepsilon \in (p^-, p^+)$, leading to the fully stochastic regime described above. See [10] for a more complete discussion of the behaviour of f_σ in the limit of small and large σ.

3 Modelling uncertainties

In this section we discuss the modelling of two specific sources of vibro-acoustic uncertainty within the stochastic evolution operator framework presented above. We describe the modelling of (i) uncertain/rough surface reflections and (ii) uncertainties in the location of a point source driving the system.

3.1 Uncertain reflections

Uncertain or rough surface reflections may be modelled using the PDF (6) by modifying the parameter σ_2. The spatial integral in (1) may be computed analytically for polygonal domains and remains bounded on setting $\sigma_1 = 0$, hence in this work we take $\sigma_1 = 0$ and consider the influence of the parameter σ_2 alone. The directionally dependent part of our PDF becomes equivalent to the bidirectional reflectance distribution function (BRDF) used in ray tracing for computer graphics [3]. Models based on a linear combination of diffuse and specular reflections are typically applied for applications in acoustics [3], which in our notation corresponds to using the operator

$$\alpha \mathscr{L}_{(0,\infty)} + (1-\alpha)\mathscr{L}_{(0,0)} \tag{8}$$

in place of $\mathscr{L}_{(0,\sigma_2)}$, where $\alpha \in (0,1)$ is a scattering coefficient. The shape of the distribution given by $\mathscr{L}_{(0,\sigma_2)}$ resembles a smoothed version of (8), where a relatively large value of σ_2 will lead to a similar model as a choice of α close to 1, and a relatively small value of σ_2 close to zero will give similar results to a choice of α close to zero. In general, an approximate correspondence between the scattering coefficient α and σ_2 is difficult to establish. However, we will investigate this numerically in the Sect. 4.

3.2 Uncertain sources

In this section we discuss the source terms ρ_0 used to drive the system (3). A source term arising from an uncertain boundary condition was proposed in [10] and takes the form

$$\rho_0(s,p) = \frac{\exp\left(-p^2/(2\sigma_2^2)\right)}{\sqrt{2\pi\sigma_2^2}\operatorname{erf}\left(1/(\sqrt{2}\sigma_2 c)\right)}. \tag{9}$$

For small σ_2, this corresponds to a unit boundary density propagating (on average) in the direction $p = 0$, that is, in the direction of the interior unit normal vector $\hat{\mathbf{n}}$ at s. For large σ_2 it corresponds to randomly directed propagation from the boundary. Such a condition may be applied for all $s \in \Gamma$, or on a subset of Γ as in [10]. Here a homogeneous Neumann boundary condition was assumed over the rest of the boundary Γ.

We will also consider an excitation from a point source with an uncertain location. The energy density on the boundary ρ_0 arising from an acoustic velocity potential point source with an exactly known location $\mathbf{r}_0^* = (x_0^*, y_0^*)$ and angular frequency ω is given by [11]

$$\rho_0(s,p;\mathbf{r}_0^*) = \frac{\omega\rho^f \cos(\vartheta(s,\mathbf{r}_0^*))\delta(p-p_0^*)}{8\pi|\mathbf{r}_s - \mathbf{r}_0^*|}. \tag{10}$$

Here ρ^f is the density of the fluid medium and $\vartheta(s,\mathbf{r}_0^*)$ is the minus the angle that the vector from $\mathbf{r}_0^* \in \Omega$ to $s \in \Gamma$ makes with the interior unit normal vector $\hat{\mathbf{n}} = (n_x, n_y)$ at s. In addition, $\mathbf{r}_s = (x,y)$ are the Cartesian coordinates of the point $s \in \Gamma$ and $p_0^* = \sin(\vartheta(s,\mathbf{r}_0^*))/c$ is the tangential component of the slowness vector at $s \in \Gamma$ due to the ray trajectory arriving from $\mathbf{r}_0^*$.

We generalise the deterministic point source described above to a stochastic one by considering a disc D_R with centre $\mathbf{r}_0^*$ and radius R chosen such that $D_R \subset \Omega$. We then replace the

source point with a scaled Gaussian probability distribution inside D_R, where the probability only depends on the radial distance $r \in [0,R)$ from $\mathbf{r}_0^*$. Explicitly, we obtain

$$\rho_0(s,p;D_R) = \frac{\omega\rho^f}{8\pi}\int_0^{2\pi}\int_0^R \frac{\cos(\vartheta(s,\mathbf{r}_0))\delta(p-p_0)}{|\mathbf{r}_s-\mathbf{r}_0|}\frac{\exp(-r^2/(2\varepsilon^2))}{2\pi\varepsilon^2(1-\exp(-R^2/(2\varepsilon^2)))}r\,\mathrm{d}r\,\mathrm{d}\phi, \tag{11}$$

where (r,ϕ) are polar coordinates in D_R that govern the location of the source point $\mathbf{r}_0 = (x_0,y_0) = (x_0^*+r\cos\phi, y_0^*+r\sin\phi)$. Also, ε is the standard deviation in the underlying Gaussian distribution before scaling and $p_0 = \sin(\vartheta(s,\mathbf{r}_0))/c$.

In order to also incorporate the uncertain surface reflection effects in Eq. (11), we replace delta distribution $\delta(p-p_0)$ by a truncated and normalized Gaussian distribution

$$\frac{\exp\left(-\dfrac{(p-p_0)^2}{2\sigma_2^2}\right)}{\sqrt{2\pi}\sigma_2\psi_{\sigma_2}(p^-,p^+)} \to \delta(p-p_0), \quad \text{as} \quad \sigma_2 \to 0, \tag{12}$$

which is analogous to those defined in (6)–(7). In the next section we will numerically investigate the influence of the parameter ε in controlling the focussing and defocussing of the source term.

4 Numerical results

In this section we describe numerical experiments based on the ideas for modelling vibro-acoustic uncertainties described above. The discretisation of the model(s) described in the Sections 2 and 3 is performed using a piecewise constant collocation method in the spatial variable s and a Nyström method for the momentum variable p. For further details, the interested reader is referred to [10]. We consider a rectangular domain $(x,y) \in (0,l)\times(0,0.25)$ where $l = 0.75$, initially with a boundary condition source of the form (9) along the left hand edge at $x = 0$. In the high frequency limit and as $\sigma_2 \to 0$, this problem possesses an analytical one-dimensional ray tracing solution

$$\rho(x) = \frac{\rho^f}{1+\eta^2/16}\frac{e^{-\mu x}+e^{-\mu(2l-x)}}{1-e^{-2\mu l}}, \tag{13}$$

where $\mu = \eta\omega/(2c)$ is a frequency-dependent dissipation rate along the rays with (hysteretic) loss factor η and angular frequency ω.

In the left plot of Fig. 2, we show the results of numerical simulations with the uncertain boundary condition (9) for different values of σ_2. We choose $\sigma_1 = 0$, $\omega = 200\pi$, $c = 1$, $\rho^f = 1$ and $\eta = 0.01$. After computing the density inside the rectangle, we average over the y-coordinate for ten subregions of the segment $(0,0.75)$. We plot the natural logarithm of the averaged density. The numerical results demonstrate that the simulation with $\sigma_2 = 0.01$ provides a good agreement with the exact ray tracing solution (13), that is, the limiting case when $\sigma_2 \to 0$. In addition, a good agreement between the numerical results with $\sigma_2 = 10$ and $\sigma_2 = 100$ indicates that the fully stochastic regime has been achieved by these parameter values. Note that the

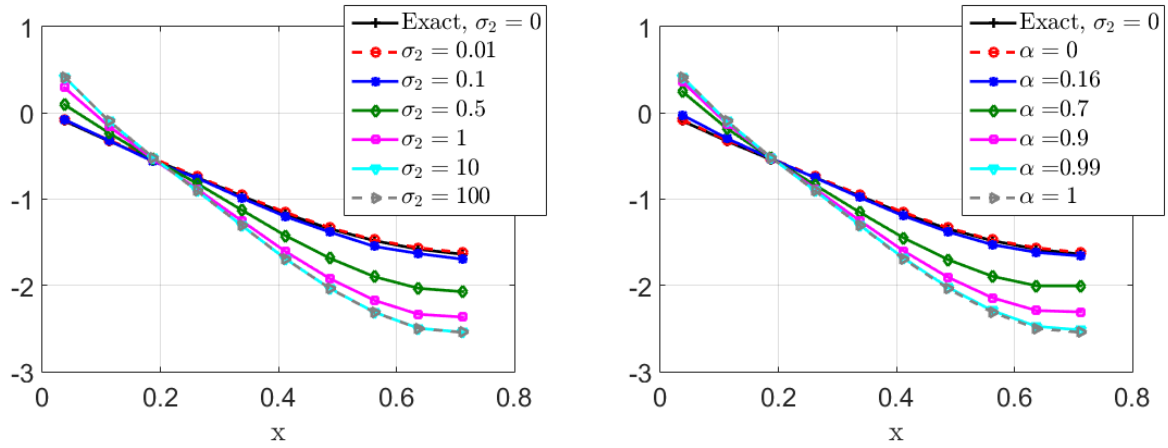

Figure 2: **Numerical simulation on rectangle $(x,y) \in (0,0.75) \times (0,0.25)$ with an uncertain boundary source at $x = 0$; logarithm of the interior density averaged over y-coordinate. Left: numerical solutions with different values of σ_2. Right: linear combination operator $\alpha\mathscr{L}_{(0,100)} + (1-\alpha)\mathscr{L}_{(0,0.01)}$ solutions for different values of α. Parameter values: $\sigma_1 = 0$, $\omega = 200\pi$, $c = 1$, $\rho^f = 1$ and $\eta = 0.01$.**

decrease in the energy density close to $x = 0.75$ for larger values of σ_2 is due to an increased number of reflections between the upper and lower edges close to the boundary source.

In order to compare our numerical results with the more standard rough surface scattering model (8), we approximate the operator (8) using

$$\alpha\mathscr{L}_{(0,100)} + (1-\alpha)\mathscr{L}_{(0,0.01)}$$

and perform numerical simulations for different values of α; see the right plot of Fig. 2. Results for a range of α values are plotted, which give qualitatively similar results to the left plot where the dependence of the solution on the parameter σ_2 was considered. Note that in both cases, the numerical solutions for different values of α or σ_2 interpolate between the purely deterministic solution, i.e. when $\alpha = 0$ or $\sigma_2 \to 0$, and the purely stochastic solution when $\alpha = 1$ or $\sigma_2 \to \infty$.

We now consider numerical experiments with an uncertain point source of the form (11)–(12), see Fig. 3. We use the same rectangular domain as above and take the same parameter values: $\sigma_1 = 0$, $\omega = 200\pi$, $c = 1$, $\rho^f = 1$ and $\eta = 0.01$. In Fig. 3, a disc D_R with radius $R = 0.05$ and centre $\mathbf{r}_0^* = (0.2, 0.1)$ is represented by a black circle with a star at the centre. We display four numerical results for different values of σ_2 and ε. For visualization purposes, we triangulate the domain and plot the logarithm of the interior density computed at the centroids of each triangle. We consider two values for σ_2, that is, approximately specular reflections ($\sigma_2 = 0.01$) and approximately diffuse reflections ($\sigma_2 = 10$). Similarly, we consider the same two values for ε.

The upper left plot of Fig. 3 shows the interior density corresponding closely to the deterministic problem with approximately specular reflections at the boundaries and a localised source point

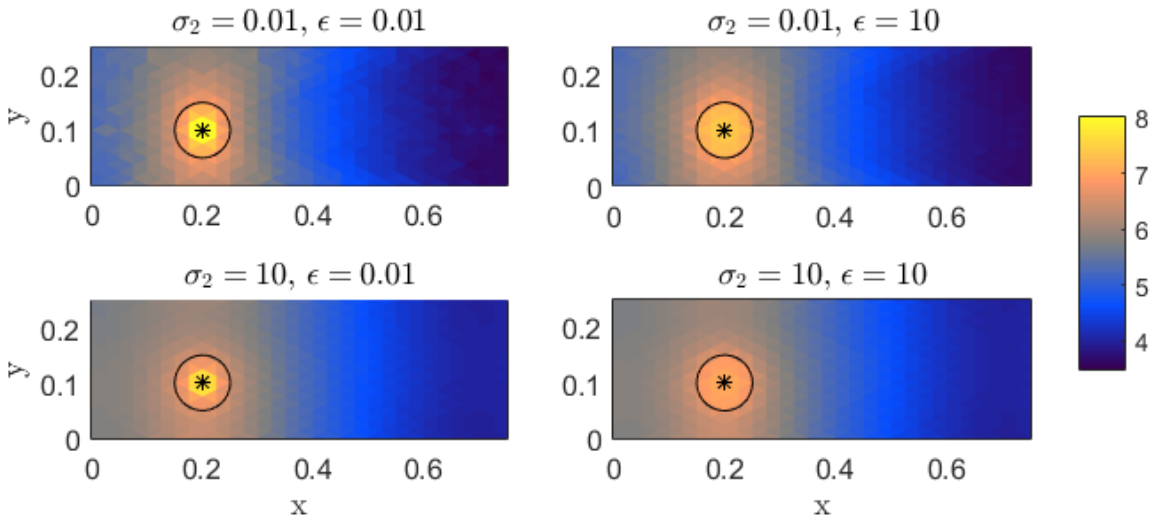

Figure 3: **Energy density distributions in the presence of uncertain reflections and a source point modelled by the parameter values of σ_2 and ε. A disc D_R of the uncertain source with radius $R = 0.05$ and centre $(0.2, 0.1)$ is indicated by the black circle with a star at the centre. The colour bar indicates the logarithm of the interior density computed on a triangulation of the domain at the centroids. Parameter values: $\sigma_1 = 0$, $\omega = 200\pi$, $c = 1$, $\rho^f = 1$ and $\eta = 0.01$.**

distribution concentrated at $\mathbf{r}_0^*$. The upper right plot of Fig. 3 shows the effect of increasing the parameter ε corresponding to an increased level of uncertainty regarding the location of the source point. The result clearly illustrates that the energy density is now spread more evenly over the disc D_R, rather than concentrated at the centre. The lower left plot of Fig. 3 demonstrates the solution obtained when the location of the source point is known with a high probability, but with approximately diffuse reflections at the boundaries. Here one clearly sees the influence of the source point at the centre of D_R, but the diffuse boundary reflections lead to a smoother energy density distribution across the whole domain compared to the upper left plot of Fig. 3. Finally, the lower right plot of Fig. 3 shows numerical simulation with diffuse reflections at the boundaries and an uncertain source point located inside the disc D_R. As expected, the result combines the features observed in the upper right and lower left plots, that is a more smoothly distributed solution globally, and a defocussed source term. Notice the significant difference in the energy density distribution between upper left and the lower right plots of Fig. 3.

5 Conclusions

We have described a framework for modelling uncertain high-frequency vibro-acoustic problems using stochastic boundary transfer operator methods. In particular, we have considered the application of these methods to model uncertain reflections and uncertain source terms. In the former case, we have demonstrated that a direct application of our model can give qual-

itatively similar results to a more standard rough surface scattering model based on a linear combination of terms due to diffuse and specular reflections. Furthermore, our approach can easily be modified to the form of this more standard model if desired. In the latter case, we have demonstrated that an uncertain source location can be modelled leading to focussing/defocussing of the source. Our future work will consider the efficient numerical implementation of these models and their application to complex built-up systems.

Acknowledgements

Support from the EPSRC (grant no. EP/M027201/1) and the EU (FP7-PEOPLE-2013-IAPP grant no. 612237 (MHiVec)) is gratefully acknowledged.

References

[1] Kayija, J.T. The rendering equation. Proceedings of SIGGRAPH 1986: 143, DOI:10.1145/15922.15902.

[2] Le Bot, A. Energy exchange in uncorrelated ray fields of vibroacoustics, J. Acoust. Soc. Amer., Vol. 120(3), 2006, pp 1194-1208.

[3] Siltanen, S.; Lokki, T.; Kiminki, S.; Savioja, L. The room acoustic rendering equation, J. Acoust. Soc. Amer., Vol 122, 2007, pp 1624–1635.

[4] Tanner, G. Dynamical energy analysis - Determining wave energy distributions in vibro-acoustical structures in the high-frequency regime, J. Sound. Vib., Vol. 320, 2009, pp 1023-1038.

[5] Tanner, G.; Chappell, D.J.; Löchel D.; Søndergaard N. Discrete Flow Mapping: a mesh based simulation tool for mid-to-high frequency vibro-acoustic excitation of complex automotive structures, SAE Int. J. Passeng. Cars - Mech. Syst., Vol. 7(3), 2014, 2014-01-2079.

[6] Cvitanović, P.; Dettmann, C.; Mainieri, R.; Vattay, G. Trace formulas for stochastic evolution operators: weak noise perturbation theory, J. Stat. Phys., Vol. 93, 1998, pp 981-999.

[7] Lippolis, D.; Cvitanović, P. How well can one resolve the state space of a chaotic map?, Phys. Rev. Lett., Vol. 104, 2010, 014101.

[8] Celani, A.; Cencini M.; Mazzino A.; Vergassola M. Active and passive fields face to face, New Journal of Physics, Vol. 6, 2004, 72.

[9] Sommer, M.; Reich, S. Phase-space volume conservation under space and time discretization schemes for the shallow-water equations, Monthly Weather Review, Vol. 138, 2010, pp 4229-4236.

[10] Chappell, D.J.; Tanner, G. A boundary integral formalism for stochastic ray tracing in billiards, Chaos, Vol. 24(4), 2014, 043147.

[11] Chappell, D.J.; Tanner G. Solving the stationary Liouville Equation via a boundary element method, J. Comp. Phys., Vol. 234, 2013, 487-498.